Automation of Inspection for Weld†

– Fundamental Consideration –

Katsunori INOUE* and Masatoshi SAKAI**

Abstract

As an example for automation of inspection, the automatic recognition of the weld defects is made by the computer image processing and successful result is obtained.

KEY WORDS: (Weld Inspection) (Automation) (Radiography) (Computer Image Processing) (Pattern Matching)

1. Introduction

Factory automation demands automation of an inspection system following completion of automation of manufacturing processes. Automation of inspection usually includes a larger variety of difficult problems than that of manufacturing. Inspection of manufactured products must be made for a small quantity of defective products from the plentifulness of products. One of the problems in automation of inspection is how to incorporate a discriminant standard in an automatic device for recognition of defects. Manual inspection is achieved by comprehensive and elastic standards based on the past experience of inspectors, mechanism by which defects occur and comparison with a standard quality. Another problem is a large diversity of the site and morphology of defects. Depending on the kind of product or the process of manufacture, the sites of defect may be limited or predictable. However, in most industrial fields, the site and morphology of defects are almost always irregular. This means that inspection deals with indefinite objects that have indeterminate properties and that are unknown where to exist. It is necessary to choose sensors suited for such objects and provide a performance environment to these sensors. Furthermore, for processing of inspection, the choice of sensors matched to the process and effective processing of sensor output are important.

Non-destructive inspections of weld joint include visual inspection, transmission radiography, ultrasonography, magnetic particle inspection, penetration inspection, electromagnetic induction inspection and acoustic emission inspection[1]. Defects to be detected by these inspection methods are of indefinite nature. Visual inspection of beads may be an example of most simple inspections in welding. However, faulty beads are not categorized by morphological definition but occur in various parts of beads and in various forms such as meandering, hamping, undercutting, overlapping and cracking simultaneously or separately to different degrees. Effective automatic recognition of such indefinite objects and automatic incorporation of a discriminant standard into an automatic inspection device are needed for automation of an inspection system.

2. Recognition of Indefinite Objects

2.1 Recognition of indefinite objects and application of image processing technique

Of various methods for inspection of weld joints described previously, X-ray transmission, magnetic particle and penetration inspections are mediated by human visual information. Generally, human visual sense may be replaced by an image-pickup device such as an ITV camera as a sensor for automation. This report deals with such an inspection method. More concretely, an object of inspection is picked up by an ITV camera. After digital conversion, the image data are put into a computer, and after various stages of processing, necessary information is selectively extracted. This is an application of so-called

† Received on May 31, 1985
* Professor
** Graduate Student

Transactions of JWRI is published by Welding Research Institute of Osaka University, Ibaraki, Osaka 567, Japan

computer-image processing technique.

As already described, objects to be detected are variable locationaly as well as morphologically. In image processing, it requires an effective enhancement process for separation of the object from the background in the first stage. Filtering may be used for this purpose, but there is a problem of setting each element of filtering operators. In this study, a learning process was introduced to solve the problem.

2.2 Introduction of learning process

Setting of above-described filtering operators corresponds to institution of a previously mentioned discriminant standard used in manual inspection for selecting defectless and defective products. It should be based on extensive knowledge on the occurrence of defects. At least, defects should be thoroughly characterized for determining filtering operators.

In an automatic inspection system, construction of a learning system is required so that defect characteristics are automatically discerned. By feeding various kinds of defect signals into an automatic device, the defect characteristics are automatically profiled and systematically recorded. A discriminant standard, namely, each element of filtering operators, may be determined on the basis of the results of this learning process.

An experimental application of this system is described in the following of the report.

3. Characteristics of Defect Image and Its Processing

3.1 An example of indefinite objects – Defects in X-ray radiograph

X-ray radiography of weld joint is a typical visual inspection. So, this method is exclusively dealt with as a test case in this study.

Studies on automatic inspection of radiography have so far been reported[2-6]. However, the difficulty in the automatic inspection has not completely overcome.

Defects detected by radiography test include the following.

a) Blowhole
b) Pipe
c) Slag inclusion
d) Lack of fusion
e) Incomplete penetration
f) Cracking

These defects may be roughly divided into 2 types by their morphology; isolated dot-like type and continued linear type. As the latter is comparatively easily identified, isolated dot-like type of defects is chiefly studied. Furthermore, of isolated dot-like defects, the blowhole is only dealt with because of its high frequency appearance.

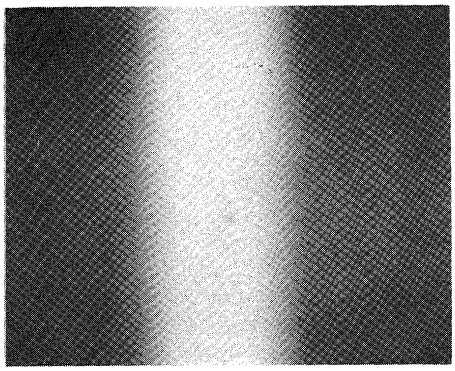

Fig. 1 An example of X-ray radiograph on TV monitor.

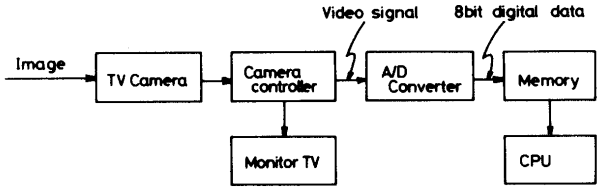

Fig. 2 Block diagram of image processing system.

Figure 1 shows an example of the radiograph of the weld which includes blowhole. **Figure 2** shows a block diagram of the system that processes such an image. This image processing system produces digital image data of 256 x 256 pixels, 8 bits, from the output signal of a TV camera (Hamamatsu Photonics C-1000). Various data processing is achieved in CPU. A block diagram of CPU-connected peripheral devices is shown in **Fig. 3**. CPU is a minicomputer (MELCOM 70/30) which has a main memory of 256 KB and a hard disc of 40 MB, and is connected to the network system of the microcomputer through serial port (RS-232C). This minicomputer is used for major data processing. The microcomputer is used for only supplementary purpose. As soft ware, FORTRAN language is used under the control of UOS (Universal Operating System), which is an operating system of the minicomputer MELCOM 70/30. FROTRAN 7 used is more replenished than JIS 7000 level and allows more free access to files, so suits the purpose of this study for processing large volume of data. **Figure 4** shows an example of the horizontal scanning which expresses the density distribution, at the position of the blowhole. The density distribution is characterized as under.

(a) The central part shows a gentle, upward convex distribution of brightness due to weld reinforcement.
(b) The peripheral part of the base metal are relatively flat.

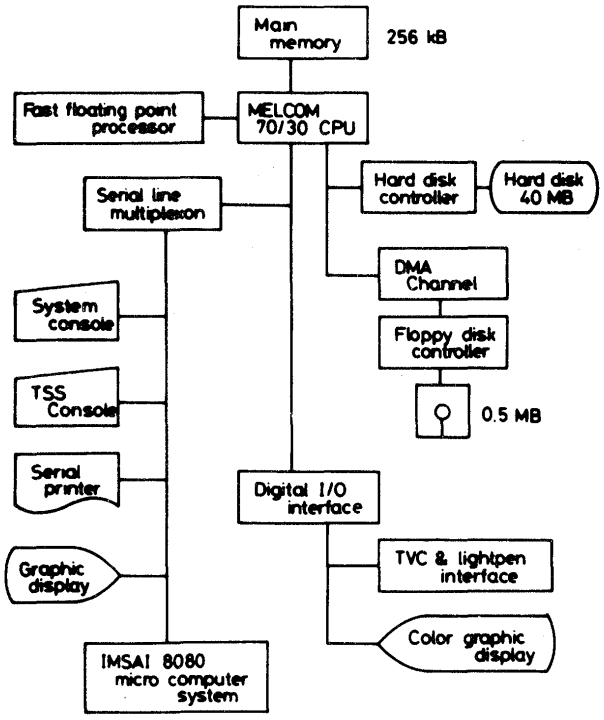

Fig. 3 Block diagram of minicomputer system.

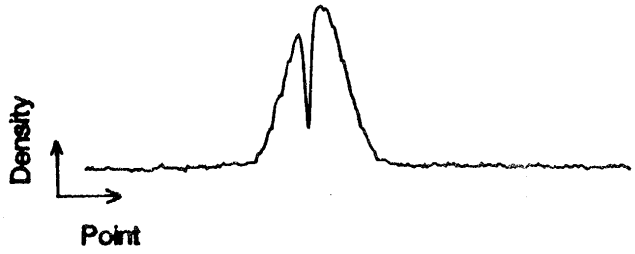

Fig. 4 Horizontal scanning data of defect position.

(c) Noise of high space-frequency is superposed over the whole region.

(d) The density change due to the defect is more pronounced than the reinforcement-induced density change and has a larger amplitude than noise.

These characteristics are used to extract the defect.

3.2 Characteristics of the defect image

A blowhole is a gas bubble generated in the molten metal in the region of weld. It is visualized as a round or oval shape. **Figure 5 (a, b)** shows 2 examples of blowhole

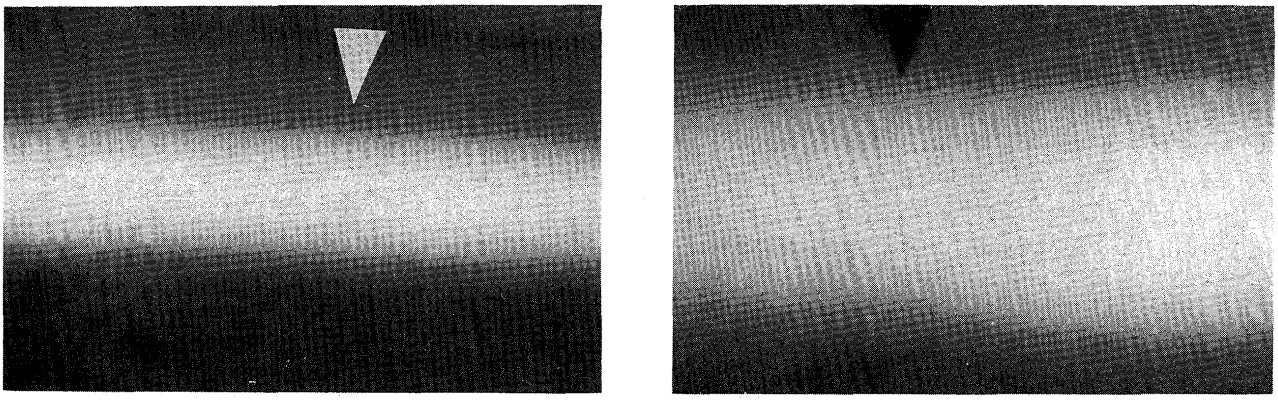

(a) (b)

Fig. 5 (a), (b) Examples of X-ray radiographs including defects.

141	143	142	143	141	143	142	143	143	143
143	143	143	142	142	143	140	143	141	143
144	143	141	143	142	142	142	143	142	143
144	140	137	138	133	138	137	142	143	143
141	142	134	130	125	127	136	142	144	147
144	143	137	130	122	127	132	142	143	146
146	146	142	136	131	131	136	143	143	147
145	143	143	143	141	141	140	143	142	145
148	146	147	143	143	143	143	147	146	147
147	143	143	146	143	143	143	143	145	147

(a)

105	105	106	104	106	104	106	104	105	104
105	105	106	104	105	103	104	104	105	105
106	106	106	103	104	104	105	104	105	106
105	105	106	103	105	102	104	103	105	105
107	106	106	102	103	101	104	103	105	105
106	105	106	102	104	103	105	104	105	105
107	106	106	104	105	104	104	105	105	106
106	105	106	104	105	105	105	105	106	106
107	106	107	106	105	105	106	106	106	105
106	106	107	105	106	105	107	105	106	106

(b)

Fig. 6 (a), (b) Examples of image data of blowholes.

3	2	2	2	2	2	2	2	2	3
3	2	2	2	1	1	1	2	2	3
3	2	1	-1	-2	-2	0	1	2	3
2	1	-2	-5	-7	-7	-4	-1	1	3
2	0	-4	-8	-11	-11	-7	-2	1	2
2	0	-3	-8	-10	-10	-7	-2	1	3
3	2	-1	-4	-6	-5	-3	0	2	3
3	3	1	0	0	0	0	2	3	4
4	3	3	2	2	2	2	3	3	4
4	4	3	3	3	3	3	3	3	4

(a)

1	1	2	0	2	0	2	0	1	0
1	1	2	0	1	-1	0	0	1	1
2	2	2	-1	0	0	1	0	1	1
1	1	2	-1	1	-2	0	-1	1	1
3	2	2	-2	-1	-3	0	-1	1	1
2	1	2	-2	0	-1	1	0	1	1
3	2	2	0	1	0	0	1	1	2
2	1	2	0	1	1	1	1	2	2
3	2	3	2	1	1	2	2	2	1
2	2	3	1	2	1	3	1	2	2

(b)

Fig. 7 (a), (b) Examples of image data of blowholes after bias canceling.

of the X-ray radiograph picked up by the TV camera and displayed on the monitor (Fig. 5a, b). **Figure 6 (a, b)** shows the digital-converted 10 x 10 data of the blowhole image of Fig. 5. **Figure 7 (a, b)** shows the bias-cancelled (described later) results. The digital data in Figs. 6 and 7 show larger differences between (a) and (b) than is seen in Fig. 5. In (b), the density change is far less than in the peripheral region. Thus, for automatic recognition of images with less brightness change, simple enhancement techniques such as made by common-place differential operator are not effective, because of the presence of overall density unevenness and difficulty in discrimination from noise. Thus a filtering process with matching patterns becomes necessary.

3.3 Collection and filing of defect patterns

Collection of a large amount of defect patterns is needed for preparation of the matching pattern. A large number of X-ray radiographic films which contain blowhole images discriminatively identified by qualified inspectors were first obtained. Each picture was placed on the illuminator and taken with the TV camera for recording as the data of blowhole. The data consisted of 10 x 10 pixels, and the window was adjusted to the size of 18 x 18 mm and the magnification of the TV camera was accordingly adjusted so that the pixels had a size of 0.18 mm each. In actual recording of defect pattern, optimal location for the sampling was determined from the image on the monitor and recorded by using a light-pen. In this procedure, the absolute brightness of the pattern was disregarded and the sensitivity of the TV camera and lens opening were so adjusted as to obtain the maximum contrast between the defect and surrounding background. The data thus collected, if not further refined, still contain constant bias components superposed over defect information. For effective achievement of subsequent processing, these disturbing bias components should be eliminated to increase the dynamic range of the data. Bias cancel operation was then made by subtracting the mean value of 10 x 10 pixels from the original data. Bias cancellation is schematized in **Fig. 8**. As seen in

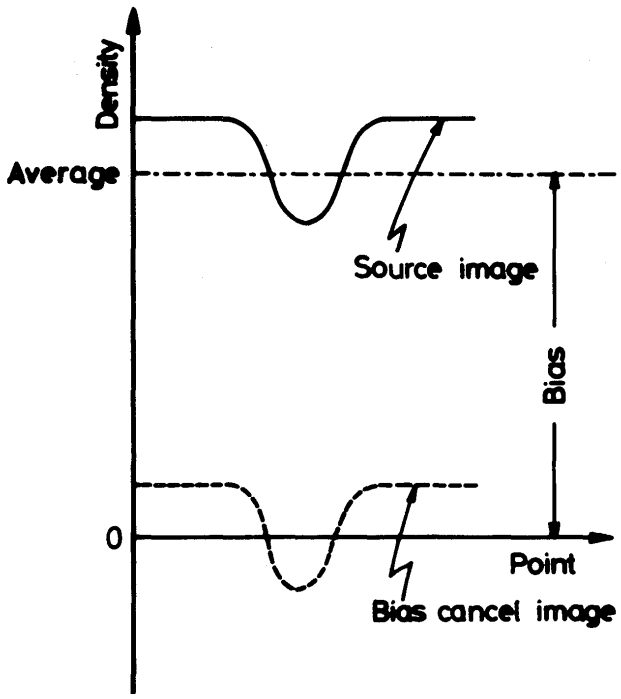

Fig. 8 Illustration of average bias canceling.

Fig. 7(a, b), the total sum of the 10 x 10 pixel data approached to 0 by this procedure, which provides an advantage to a subsequent filtering process.

The defect data thus collected and processed were stored in a external memory (hard disc) as a data file to

facilitate subsequent processes. Each data file consists of 15 records. Each record is a random access file of 256 bytes. Information stored in each record represents one kind of defect. Two hundred bytes are allocated for pattern data information (2 bytes/datum, 2 x 10 x 10 = 200) and remaining 56 bytes are reserved for auxiliary information such as the installation condition of the TV camera, labelling of the X-ray photographs and the date of recording. Such auxiliary information permits easily refrieving the desired defect pattern from the random access files and, in a way, constitutes a kind of data base of weld defect.

3.4 Catagorization of defect patterns by similarity

The concept of similarity is introduced for categorization of the defect patterns recorded and stored in file by the above-mentioned process. Similarity is a concept that expresses equality between 2 pattern vectors in a pattern feature space. Assuming that the defect pattern is 10 x 10 matrix $\mathbf{F} = \{F_{i,j}\}$ (i, j = 1 . . . 10), it can be regarded to be a 100-dimensional vector as expressed in the following equation.

$$\mathbf{f} = \{f_k\}$$
$$= \{F_{i,j}\} \ (k = 1 \ldots 100, k = 10(i-1)+j) \quad (1)$$

Letting an unknown pattern vector of the same dimension (100-dimension) be $\mathbf{g} = \{g_i\}$ (i = 1 . . . 100), similarity S of vectors **f** and **g** is expressed as

$$S(\mathbf{f}, \mathbf{g}) = \frac{(\mathbf{f} \cdot \mathbf{g})}{(|\mathbf{f}| \cdot |\mathbf{g}|)} = \frac{\sum_{i=1}^{100} f_i \cdot g_i}{(\sum_{i=1}^{100} f_i^2)^{1/2} (\sum_{i=1}^{100} g_i^2)^{1/2}} = \cos\theta \quad (2)$$

In other words, S is a direction cosine of **f** to **g**, where $-1 \leqq S \leqq 1$ and S = 1 when $\mathbf{f} = c \cdot \mathbf{g}$ (c is a constant).

The interrelation of the filed defect data was now analyzed using S. All the 108 defect data were arranged in all sorts of combination to calculate S for respective combinations. The total combinations amounted to ${}_{108}C_2 = 5778$. The frequency of S is shown in a histogram as **Fig. 9**. For the sake of comparison, this figure also shows the frequency of S calculated for the data processed by mode cancellation using the density mode of of the original 10 x 10 data instead of previously described bias cancellation using the mean value. Despite some differences between them, the frequency peak exists close to S(= cosθ) = 1 in both cases, indicating the presence of many distributed components in the vicinity of this region. This also indicates that there are many

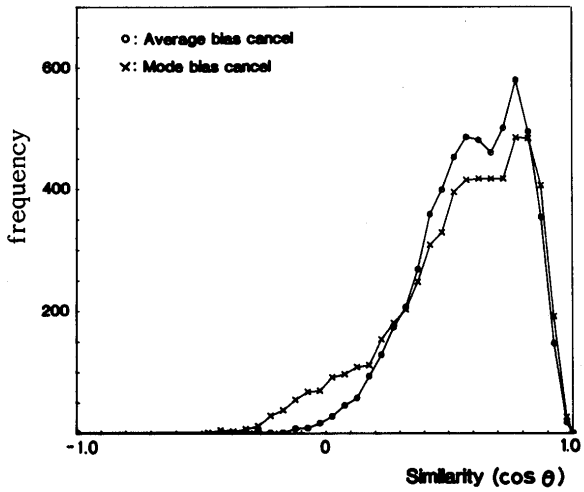

Fig. 9 Histogram of similarity for all combination of defect data.

3	3	2	2	2	2	2	2	3	3
3	3	2	2	1	1	1	2	2	3
3	2	1	-1	-3	-2	-1	1	2	3
3	1	-2	-6	-9	-8	-1	1	2	3
3	0	-5	-10	-14	-14	-9	-3	1	3
3	0	-4	-10	-13	-12	-8	-3	1	3
3	2	-1	-5	-7	-7	-4	0	2	4
4	3	1	0	-1	-1	0	2	3	4
4	4	3	2	2	2	3	3	4	4
4	4	4	3	3	3	4	4	4	4

Fig. 10 Data of Filter No. 2.

morphologically similar defect patterns. However, the presence of distributed components in the vicinity of S = 0 shows that there are also defect patterns that have considerably different density distribution.

Similarity of each datum to some typical patterns was then determined. To prepare the typical pattern, the average value of the 108 defect data was calculated. This is shown in **Fig. 10**. The matrix of this mean value and similarity of each defect pattern were obtained and shown in a histogram as is shown in **Fig. 11**. It is noted that approximately half, i.e., 60, of the data is in the range of $\cos\theta \geqq 0.8$. This justifies the data of Fig. 10 to be regarded as a standard pattern of the defect. The defect data may also be categorized on the basis of S.

3.5 Filter specifically matched to defect patterns

A differential filter or Laplacian (second order differential) operator is generally used for enhancement of the part where the density changes rapidly such as a defect pattern. However, since these kinds of filter simultaneously enhances other factors than the image of the defect, such as noise, the images of base metal and reinforcement

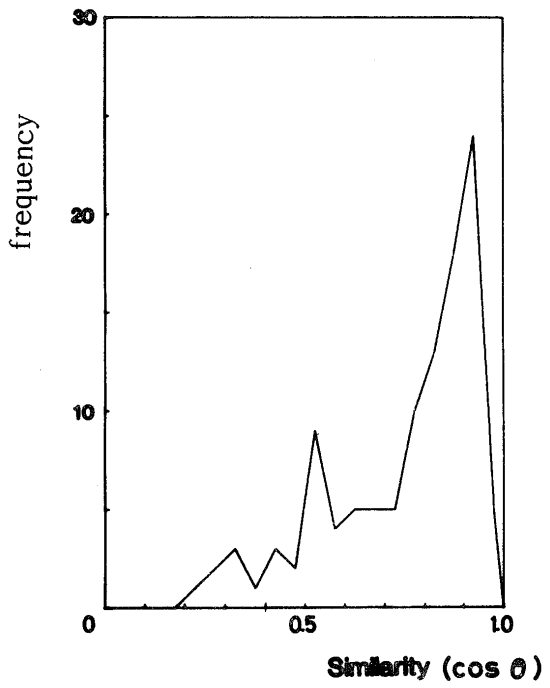

Fig. 11 Histogram of similarity to Filter No. 2.

boundary, a filter that selectively enhances the desired object only should be used. It is a technique called matching filtration. If the original pattern is expressed as function f(i, j) (it indicates the density at point (i. j)) and the feature of the object as function g(k, l), by calculating the cross correlation between f and g at each point of the original pattern, only the part that shows a similar property to g in f produces a pronounced response and gains enhancement. The cross correlation is obtained by the following two-dimensional convolusion.

$$F(i,j) = \sum_{k=-m}^{m} \cdot \sum_{l=-n}^{n} f(i+k, j+1) \cdot g(k,l) \qquad (3)$$

This equation is nothing but the calculation of the similarity of **Eq.(2)** without normalization. Here g is called a matching filter. The filter g is more desirable if produced from the typical pattern of the defects. Three kinds of matching filters were then tested.

As shown in **Fig. 12**, the 1st one is a kind of Laplacian operator artificially simulated to the shape of the defect. The size of K_2, L_2 almost equals the size of the defect portion in the mean matrix shown in Fig. 10. The total sum of the elements of the matrix (1 or −3) becomes 0. This is called Filter No. 1.

As the 2nd filter, the averaveraged matrix itself (Fig. 10) was used on the basis of the concept that this is one of the patterns that represent the defect. This is called Filter No. 2.

The 3rd one is a filter that compensates the shortcomings of the mean matrix pattern. As shown in Fig. 9,

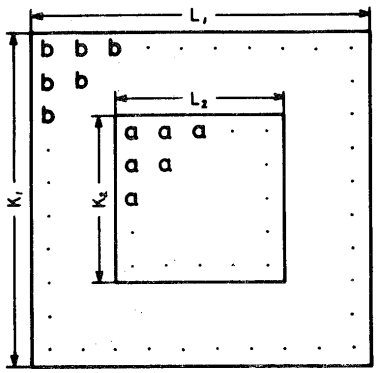

$K_1 = L_1 = 10$
$K_2 = L_2 = 5$
a = -3
b = 1

Fig. 12 Illustration of Laplacian filter artificially simulated to shape of defect; Filter No. 1.

the histogram of mutual similarity of the defect, and in Fig. 10, the histogram of similarity to the mean matrix pattern, some defects have the feature that diverts largely from those of other defects (corresponding to the small values of $S(=\cos\theta)$ of Figs. 9 and 10). Since the mean pattern contains a co-mixture of the features of the minority group of defects, the characteristics of typical defect pattern might be somewhat lost in the mean defect pattern. The following correction was, therefore, attempted to obtain a filter that more precisely reflects similarity. **Table 1** has been prepared from the mutual similarity of the defect data. The upper equation in Table 1 is used for calculation of similarity between defects K and L. In this equation, threshold (= 0.6) was introduced and the I_{KL} value was determined as shown in the Table. This value is an index to identify the similarity between defects K and L. This index was then calculated for all the data and summed up for all the combinations. The data number M for maximum ΣI_{KL} was obtained, and the mean value of only the data that have similarity to defect data M was calculated by **Eq.(4)**.

$$g = \sum_{K=1}^{N} AK \cdot I_{KM}/nM \qquad (4)$$

Furthermore, some modification was made for g by adjusting the peripheral elements of matrix so as to make summation of all the elements to zero. This may be regarded to be a similarity-reflected matching filter. **Figure 13** shows the matrix of Filter No. 3.

The criterion for evaluating the filter-produced enhancement effects were then formulated. **Figure 14** shows an example of the enhanced data F(i, j) (j = 1 ... 256) on a certain horizontal scanning line. The peak marked "signal" corresponds to the signal of the defect and "noise" to the signal of the background. The S/N ratio was then obtained by the following equation.

$$S/N = 20 \log_{10}(D - M)/(N - M) \qquad (5)$$

, where D; maximum level of defect signal, N; maximum

Table 1 Calculation method to obtain similarity reflected matching filter.

$$\cos\theta_{KL} = \frac{\sum^{K} a_{ij} \cdot a_{ij}}{\left\{\sum^{K} a_{ij}^2\right\}^{1/2} \cdot \left\{\sum^{L} a_{ij}^2\right\}^{1/2}}$$

$$I(K) = \begin{cases} 1 & (\cos\theta_{KL} \geq 0.6) \\ 0 & (\cos\theta_{KL} < 0.6) \end{cases}$$

	A1	I(1)	A2	I(2)	-------	AN	I(N)	Total of I(K)=1
A1	$\cos\theta_{11}$	1	$\cos\theta_{21}$	0	-------	$\cos\theta_{N1}$	1	n1
A2	$\cos\theta_{12}$	0	$\cos\theta_{22}$	0	-------	$\cos\theta_{N2}$	0	n2
⋮	⋮	⋮	⋮	⋮	⋮	⋮	⋮	⋮
AM	$\cos\theta_{1M}$	1	$\cos\theta_{2M}$	1	-------	$\cos\theta_{NM}$	1	nM
⋮	⋮	⋮	⋮	⋮	⋮	⋮	⋮	⋮
AN	$\cos\theta_{1N}$	1	$\cos\theta_{2N}$	0	-------	$\cos\theta_{NN}$	0	nN

$$nM = Max(n1, n2, \cdots, nN)$$

$$F = \frac{\sum_{K}^{N} AK \times I(K)}{N}$$

3	3	2	2	2	2	2	2	3	3
3	2	2	2	1	1	1	2	2	3
2	2	1	-1	-2	-2	0	1	2	2
2	1	-2	-5	-7	-7	-4	-1	1	2
2	0	-4	-8	-11	-11	-7	-2	1	2
2	0	-3	-8	-10	-10	-7	-2	1	2
2	2	-1	-4	-6	-5	-3	0	2	2
2	2	1	0	0	0	0	1	2	2
3	2	2	2	2	2	2	2	2	3
3	3	2	2	2	2	2	2	3	3

Fig. 13 Data of similarity reflected matching filter; Filter No.3.

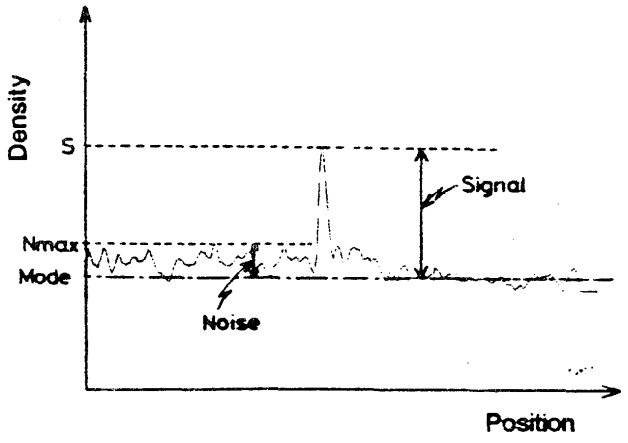

Fig. 14 Illustration for definition of S/N ratio.

level of noise and M; mode of grey level of enhanced data. The enhancement effect was quantitatively evaluated by the S/N ratio. To test the enhancement characteristics of each filter, the S/N ratio was calculated by eq.(5) after the enhancement process using 3 filters for 82 raw data. **Figure 15** shows the S/N ratio for the 3 filters. This ratio is the average value for each of the 82 cases. The results obtained are found appreciable in the order of Filters No.3, No.2 and No.1 (the hatched line part is to be explained later).

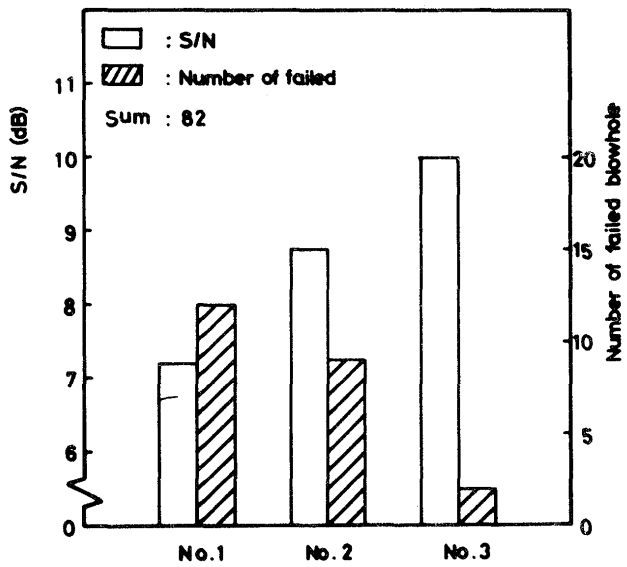

Fig. 15 Comparison of 3 kinds of filters.

Figure 16 shows an example of the enhancement effects. For the original image with 4 defects, the enhancement effects made with Filter No.2 (Fig. 16(a)) and Filter No.3 (Fig. 16(b)) are three-dimensionally displayed. Despite little change in the noise level, the 2 filters reveal a distinct difference in the processed defect signal. **Figure 17** shows an example that has 8 defects in the original pattern. The upper figure is an original image. The middle is an enhanced image with Filter No.3. The lower figure is to be explained later. **Figure 18** shows a three-dimensional display of the enhanced image. These illustrations demonstrate the effectiveness of Filter No.3 which has more similarity-reflected property.

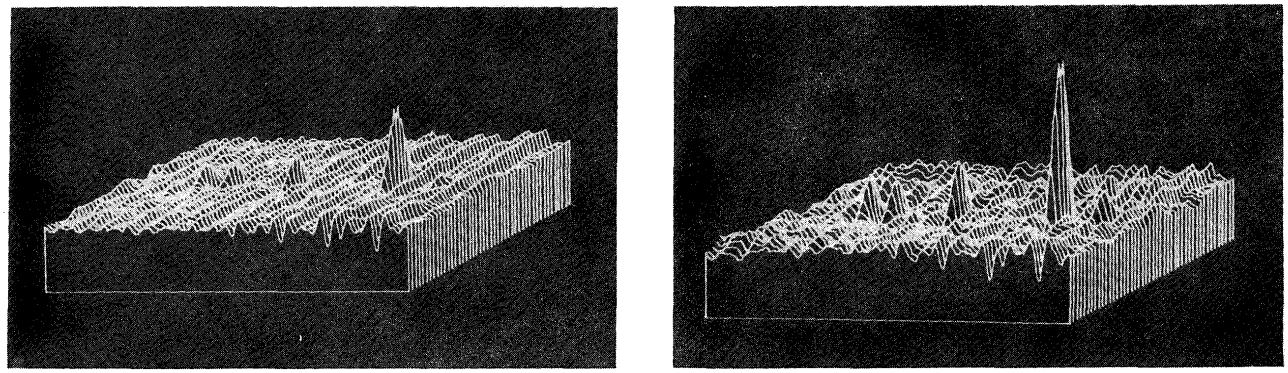

(a) (b)

Fig. 16 3-D display for enhancement of defect images by Filter No.3.

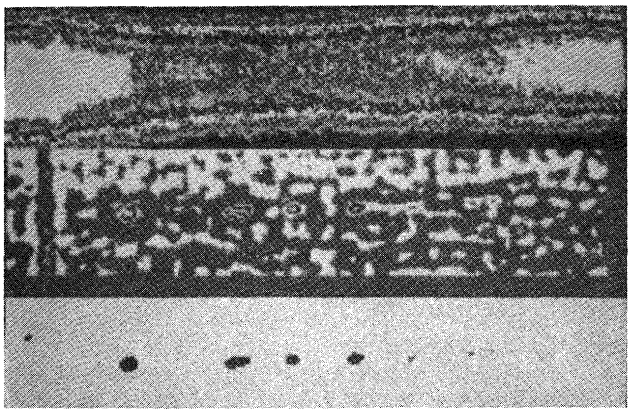

Fig. 17 An example for enhancement of 8 defect images by Filter No.3.

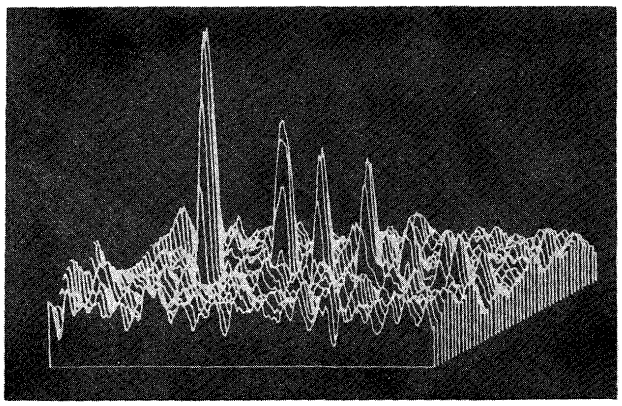

Fig. 18 3-D display for enhancement of 8 defect images by Filter No.3.

4. Automatic Recognition of Object

4.1 Preparation of the suitable filter by learning

For automatic recognition of a defect, the matching filter which is similarity sensitive as described above is prepared by test-applications to the defect data. Preparation is achieved by the following, already described procedure: (1) pickup of defect patterns and the sites of defects by qualified inspectors, (2) sampling of defect data, (3) calculation of similarity for all sampled data and (4) preparation of Filter No.3 by the above mentioned method.

This procedure should be carried out, prior to inspection, for as wide a range of defect data as possible. This operation corresponding to "learning."

4.2 Algorithmic example of automatic recognition

Firstly, using the matching filter prepared previously, the enhancement calculation is carried out by Eq.(3) for a image to be inspected.

Secondly, the presence or absence of the defect in the image is judged prior to the extraction process of the defect. This process is intended to save an unnecessary process of the defect extraction from defectless images and thus to reduce the chance of detection error. The judgement was achieved using the characteristics of the histograms of the enhancement processed image data. **Figure 19(a)** and **(b)** show the density histograms with the without defect(s) in the enhanced image data, respectively (the enhancement-processed data are hereafter called also as the density). In the histogram (b), the density distribu-

tion is more wide-spread in the highdensity region. This feature allows judgement as to the presence or absence of the defect. For this purpose, THN% is firstly calculated by **Eq. (6).**

$$THN\% = (Max - Mode)/2 \qquad (6)$$

, where Max is the maximum density and Mode is the density of the maximum frequency (refer to Fig. 16). Then the density of the data which was 100th highest the order of the density was obtained and defined as TH. In Fig. 16(a, b), it is expressed as TH1 or TH2. From this TH and THN%, the image was judged as follows:

$$\begin{aligned} &\text{with defect} \quad \text{if } THN\% \geqq TH \\ &\text{without defect} \quad \text{if } THN\% < TH. \end{aligned} \qquad (7)$$

The defect extraction process was then applied to the image judged to process the defect(s). This was performed as binarization, where setting of the threshold becomes important. The threshold was determined by the following algorithm. The data were at first arranged in order of the density. Letting the data i-th highest in density be d(i), then

$$A = \frac{d(i+5) - d(i+10)}{d(i) - d(i+5)} \qquad (8)$$

From the relation of values A and a certain value N

$$\begin{aligned} &d_{th} = d(i+5), \quad \text{if } A < N \\ &i \leftarrow i + 10 \text{ and recalculated by Eq.(8)}, \quad \text{if } A \geqq N. \end{aligned} \qquad (9)$$

The calculation was repeated from i = 1 until A < N was satisfied and d_{th} was determined. Using this d_{th}, the binarization was made for the enhanced data F(k, l) and the defect image was extracted. The above procedure is advantageous in that the binarization results do not react sensitively to the value of N. This is shown in **Fig. 20**, where the same results were obtained for both N = 0.5 – 0.7 and N = 0.3 – 0.4. On the basis of these results, N was set at 0.4 and this N value produced less detection errors.

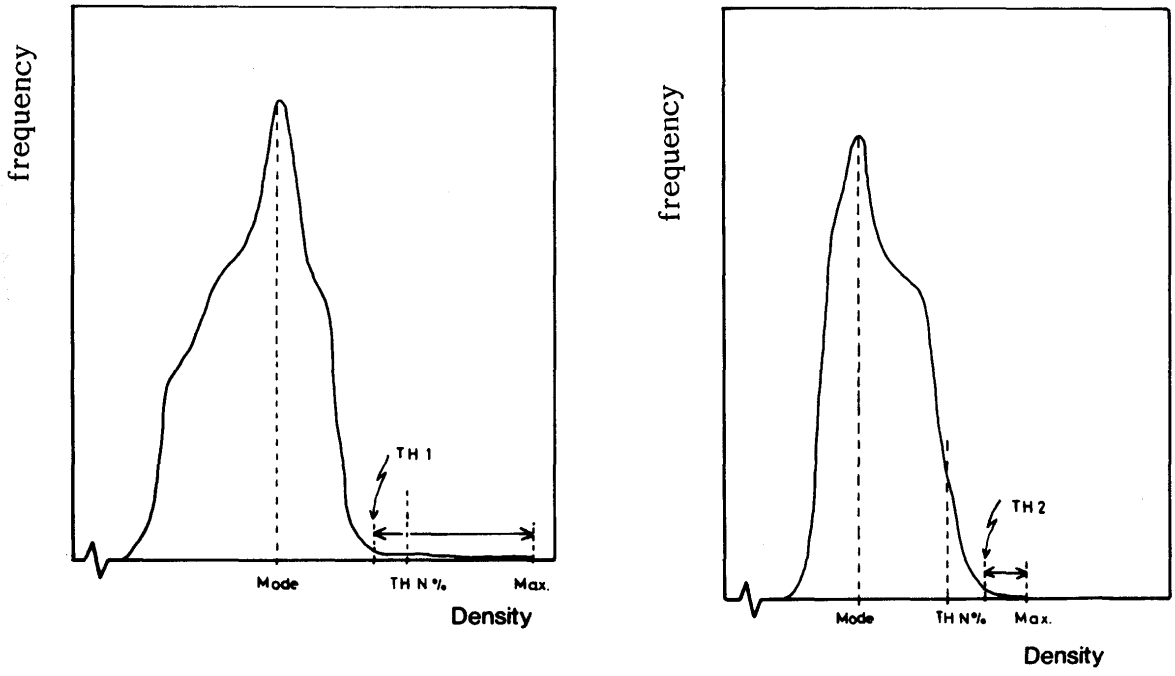

Fig. 19 Feature of histogram of pictures with and without defect images. **(a)** with defect. **(b)** without defect.

4.3 Examples of extraction process

The lower figure in Fig. 17 shows an example of defect extraction by the binarization using the algorithm described in 4.2. In this case, the 8 defects are extracted. Other examples are shown in **Figs. 21** and **22**. In both of these cases, the defects existing in the central portion are distinctly detected. Especially in Fig. 22, despite the existence of the image of the penetrameter, the detection is free from its effect. The results of this defect extraction are compared with those obtained by the visual inspection and the detection errors are determined (errors include non-detection of defect that exists and vice versa). The detection errors are shown in the hatched line part of Fig. 15. The extraction result also supports the effectiveness of Filter No. 3 that has high S/N ratio.

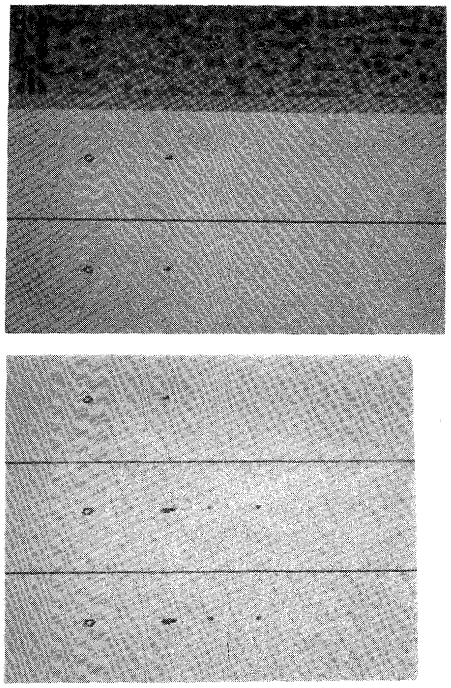

Fig. 20 Test of binarization to check dependency on N value.

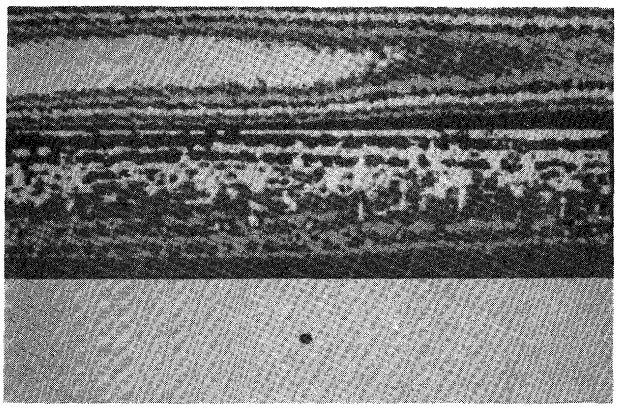

Fig. 21 An example for recognition of defect image.

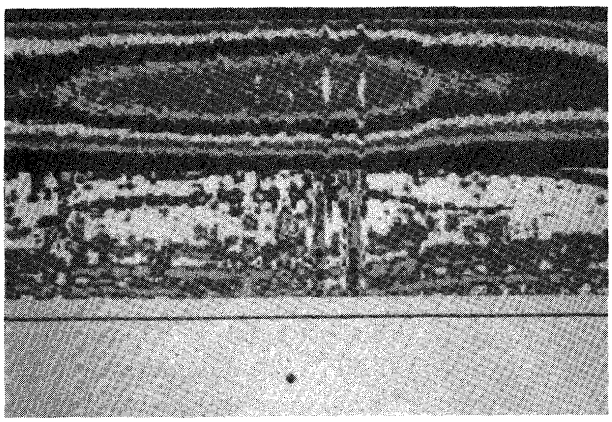

Fig. 22 An example for recognition of defect image.

5. Conclusion

This report advocated the need for identifying indefinite objects in automation of the inspection system and describes the basic method.

A system of automatically recognizable discriminant standard based on defect characterization is introduced in the pre-inspection process of learning for the defect detection from X-ray radiographs of weld joints by the image processing. Automatic recognition of defects on the basis of this standard produces successful results.

As the patterns used for automatic recognition of defects contained relatively well-defined defects, favorable results with relatively low detection error are obtained. However, for practical application, slight modification of the system is required so that ill-defined objects can also be successfully identified.

In this study, the time required for computation (almost entirely spent for the enhancement process over all the data by 2-dimensional convolusion operation) is disregarded. As convolution operation can be easily realized in hard ware technology, high speed processing with almost real time is considered possible. The method reported here may be applied not only to detect the other defects than the blowhole in the radiography, but also to perform many other visual inspections.

References

1) "Yosetsu Binran", In Japan Welding Society (The 3rd revision). (1977), Maruzen, p.1180 –– (in Japanese)

2) Y. Shirai: "Automatic Inspection of X-ray Photograph of Welding", Pattern Recognition, Vol.1 (1969), p.257–261.

3) M. Takagi and Y. Yokoi: "Yosetsubu X-senzo no Digital Shori", J. of NDI, Vol.22, No.9. (in Japanese)

4) T. Fujita, Y. Hioki and H. Matsui: "Processing of Radiographic Images of Non-Destructive Weld Testing", The Hitachi Zosen Technical Review, Vol.39 (1978), No.4, p.1–6. (in Japanese)

5) K. Inoue and M. Kobayashi: "Automatic Recognition of Weld Defects in Radiographic Test", Trans. of JWRI, Vol.11 (1982), No.2.

6) H. Koshimizu and T. Yoshida: "On a Method for Evaluating the Welding Visual Inspection Using Computer Image Processing of X-ray of Welding", JWS symposium of Fundamental and Practical Approaches to the Reliability of Welded Structures II (1982).